Journal of Engineering Mathematics **23**: 325–342, 1989.

Two-layer critical flow over a semi-circular obstruction

L.K. FORBES
Department of Mathematics, University of Queensland, St. Lucia, Queensland, 4067, Australia

Received 22 August 1988; accepted in revised form 3 April 1989

Abstract. Steady, trans-critical flow of a two-fluid system over a semi-circular cylinder on the bottom of a channel is considered. Each fluid is assumed to be inviscid and incompressible and to flow irrotationally, but the fluids have different densities, so that one flows on top of the other. Consequently, a sharp interface exists between the fluids, in addition to a free surface at the top of the upper fluid. Trans-critical flow is investigated, in which waves are absent from the system, but the upstream and downstream fluid depths differ in each fluid layer. The problem is formulated using conformal mapping and a system of three integrodifferential equations, and solved numerically with the aid of Newton's method. The free-surface shape and that of the interface are obtained along with the Froude numbers in each fluid layer. Results of computation are presented and discussed.

1. Introduction

This paper is concerned with the flow of a system of two fluids in a rectangular channel, attached to the bottom of which is a semi-circular cylinder mounted at right angles to the channel side walls. Each fluid is assumed to be ideal, in the sense that it is incompressible and inviscid and flows irrotationally, and the two fluids differ only with respect to their mass densities. Consequently, the flow exists in two distinct layers, with a free surface at the top of the upper fluid and a sharp interface separating the upper fluid from the lower fluid. To the extent that the flow is assumed ideal, boundary-layer effects are ignored at the channel side walls and along the bottom; the flow is thus identical in any plane parallel to the channel walls, and will therefore be considered as two-dimensional henceforth.

It is at once clear that a variety of possible flow situations may exist as physically admissible outcomes to such an investigation. For example, in the case of a *single* fluid layer flowing over a semi-circular obstacle, at least four different flow scenarios are known to be possible, depending upon the upstream Froude number, which is the ratio of the upstream fluid phase speed to the speed at which an infinitesimal wave travels. Two of these possibilities are discussed by Forbes and Schwartz [10] and consist of a slow-speed solution (Froude number <1) possessing a quiescent region upstream and waves downstream, and a large-speed solution (Froude number >1) which is symmetrical about the semi-circular obstacle on the channel bottom and is free from waves. A third possibility has been discovered by Vanden-Broeck [16], and is similar to the large-speed solutions discussed by Forbes and Schwartz [10], except that it is apparently a perturbation to a solitary wave, whereas the solutions of Forbes and Schwartz are perturbations to uniform flow. The fourth solution possibility is that of 'critical flow' in which there is uniform flow both upstream and downstream of the obstacle, with sub-critical flow (Froude number <1) upstream and super-critical flow (Froude number >1) downstream. This flow type is termed 'critical' since the solution of the problem using one-dimensional hydraulic theory requires that the local Froude number become exactly equal to one at the obstacle (Henderson [11]). A generaliza-

tion of this flow type to the situation in which a two-fluid system flows over an obstacle will be discussed in the present paper.

In the case of a single fluid layer flowing over an obstacle, the 'critical flow' possibility described above differs from the other types of flow in that the upstream fluid depth and phase speed cannot be specified independently in advance. A simple reason for this is provided by one-dimensional hydraulic theory, which requires that the local Froude number be exactly one at the obstacle, leading to an over-determined problem if the upstream Froude number were also specified. In some sense, then, the flow is 'controlled' by the obstacle. Several attempts have been made to compute such flows numerically, as the solution to the exact non-linear equations of inviscid free-surface hydrodynamics. For example, Aitchison [1] and Bettess and Bettess [5] used variable finite-element methods to obtain the unknown surface shape, although their techniques suffer from the drawback that the condition of uniform flow far upstream is not stipulated in advance. A more recent numerical solution which overcomes this difficulty has been given by Forbes [9], and Vanden-Broeck and Keller [17] consider this general class of flows which are controlled by a submerged weir. Critical flow solutions involving a single fluid layer have also been obtained, using various types of shallow-water approximation, by Naghdi and Vongsarnpigoon [14] and Sivakumaran, Tingsanchali and Hosking [15].

The occurrence of critical flow in a two-layer or even a multi-layer fluid system is a problem of importance in meteorology and oceanography (see Melville and Helfrich [12]), and has been considered in the context of one-dimensional hydraulic theory by Benton [4] and Wood and Lai [18], for example. Armi [2] has investigated the flow of a system of two fluids over bottom topography in a channel in which width variations may also occur, and the hydraulics of exchange flows (which involve opposite flow directions in each fluid layer) in a channel having both bottom and width variations is discussed by Armi and Farmer [3] and Farmer and Armi [6].

In this paper, a numerical method is presented for obtaining critical flow in a two-layer system, as the solution to the fully non-linear equations governing the behaviour of the two ideal fluids of different densities. The method is based upon the use of a system of three integrodifferential equations which are derived from the equations of ideal fluid flow essentially in the plane of the physical variables. The free surface and the fluid interface are treated using the arclength parametrization approach of Forbes [7] and [8], and the resulting equations are discretized and solved by Newton's method. Detailed results of computation are presented in Section 5.

2. The governing equations

We consider a system of two fluids flowing in an open channel, on the bottom of which is a semi-circular obstruction of radius R. Far upstream of the semi-circle, the flow in each layer is uniform, and the flow is everywhere subject to the downward acceleration g of gravity. We shall refer to the upper layer as 'layer 1' and the lower layer of fluid as 'layer 2'; then far upstream, layer 1 has uniform depth H_1 and fluid speed c_1 and layer 2 has depth H_2 and speed c_2. It is a feature of critical flow that conditions in both fluid layers are asymptotically uniform far upstream and far downstream, and that the upstream speeds c_1 and c_2 are unknown. If it is supposed that the uniform downstream flow speeds in layers 1 and 2 are c_1V_1 and c_2V_2 respectively, then by conservation of mass in each layer, the corresponding

uniform downstream fluid depths are H_1/V_1 and H_2/V_2. The densities of layers 1 and 2 will be denoted ρ_1 and ρ_2, respectively.

Non-dimensional variables are now introduced, by scaling all lengths relative to the quantity H_2 and all velocities relative to c_2. In these new dimensionless variables, the lower layer of fluid now has upstream speed and depth both equal to 1. A sketch of the flow in these dimensionless coordinates is given in Fig. 1. With this choice of nondimensionalization, we may define five dimensionless parameters, in terms of which solutions to this problem may be characterized. These are written $F_2 = c_2(gH_2)^{-1/2}$ which is the upstream Froude number in layer 2, $\gamma = c_1/c_2$ is a ratio of the upstream speeds in the two layers, $\lambda = H_1/H_2$ is the ratio of upstream depths, $D = \rho_1/\rho_2$ is the density ratio, and $\alpha = R/H_2$ is the dimensionless radius of the semi-circle. However, the Froude number F_2 in the lower layer and the depth ratio λ are both unknown and are therefore to be determined, as are the dimensionless downstream speed coefficients V_1 and V_2 defined above. Dimensional analysis indicates that only three of the above parameters may be specified independently, and so we give the quantities α, D and γ, and determine the constants F_2, λ, V_1 and V_2 as part of the solution. For later use, we also define another upstream Froude number $F_1 = c_1(gH_1)^{-1/2}$ in layer 1. It can be computed from the other constants according to the formula $F_1 = F_2\gamma\lambda^{-1/2}$.

The fluid in each layer is assumed to be inviscid and incompressible and to flow irrotationally. Consequently, velocity potentials ϕ_j and streamfunctions ψ_j may be defined, where the subscript j refers to the j-th fluid layer, $j = 1, 2$. If the horizontal and vertical components of the velocity vector are u_j and v_j in the j-th fluid layer, then

$$u_j = \frac{\partial\phi_j}{\partial x} = \frac{\partial\psi_j}{\partial y}\,,$$
$$v_j = \frac{\partial\phi}{\partial y} = -\frac{\partial\psi_j}{\partial x}\,, \quad j = 1, 2\,. \tag{2.1}$$

The requirement that there be no flow normal to the bottom $y = h(x)$ gives rise to the condition

$$v_2 = u_2\frac{\mathrm{d}h}{\mathrm{d}x} \quad \text{on } y = h(x)\,, \tag{2.2a}$$

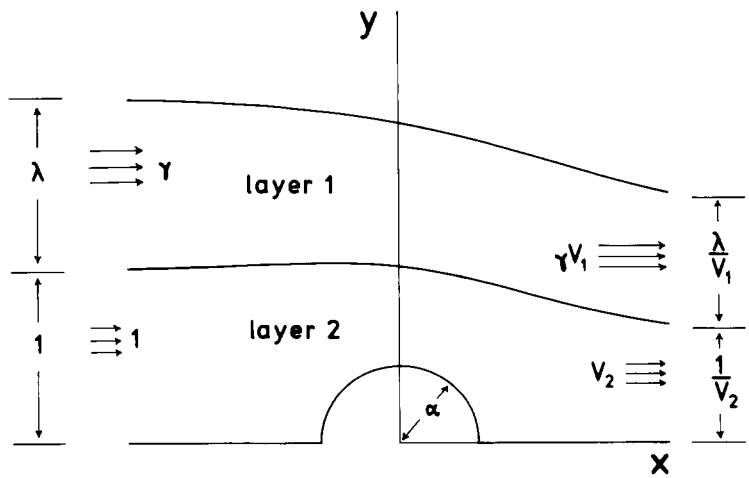

Fig. 1. Diagram of flow in dimensionless coordinates. This is a portion of an actual solution, computed with $\alpha = 0.45$, $D = 0.6$ and $\lambda = 1$ ($\gamma = 1.454$).

where

$$h(x) = \begin{cases} (\alpha^2 - x^2)^{1/2}, & \text{for } |x| \leqslant \alpha \\ 0, & \text{for } |x| \geqslant \alpha . \end{cases} \tag{2.2b}$$

If the free surface dividing the top layer of fluid (layer 1) from the air is written as $y = T(x)$, then along this surface, the Bernoulli equation

$$\tfrac{1}{2}F_2^2(u_1^2 + v_1^2) + y = \tfrac{1}{2}\gamma^2 F_2^2 + \lambda + 1 \quad \text{on } y = T(x) \tag{2.3}$$

must hold, expressing the conservation of mechanical energy within fluid layer 1, and the fact that the pressure on the surface equals atmospheric pressure. In addition, there is also a kinematic requirement that no fluid particles cross the free surface, leading to the condition

$$v_1 = u_1 \frac{\mathrm{d}T}{\mathrm{d}x} \quad \text{on } y = T(x) . \tag{2.4}$$

At any point along the interface $y = M(x)$ dividing the lower fluid from the upper, it is required that the fluid pressures on each side of the interface be equal. With the aid of Bernoulli's equation in each fluid layer, this requirement leads to the condition

$$\tfrac{1}{2}DF_2^2(u_1^2 + v_1^2) - \tfrac{1}{2}F_2^2(u_2^2 + v_2^2) + (D-1)y = \tfrac{1}{2}D\gamma^2 F_2^2 - \tfrac{1}{2}F_2^2 + D - 1 \quad \text{on } y = M(x) . \tag{2.5}$$

In addition, there are two kinematic conditions to be satisfied along the interface $y = M(x)$, expressing the fact that particles from neither fluid layer are free to cross the interface. These conditions are

$$v_j = u_j \frac{\mathrm{d}M}{\mathrm{d}x}, \quad j = 1, 2, \quad \text{on } y = M(x) . \tag{2.6}$$

Finally, it is necessary to impose explicit statements that the flow in each layer far upstream and far downstream is uniform. It is sufficient to require that the conditions

$$\begin{aligned} &u_1 \to \gamma, \quad v_1 \to 0, \quad T \to 1 + \lambda, \\ &u_2 \to 1, \quad v_2 \to 0, \quad M \to 1 \quad \text{as } x \to -\infty \end{aligned} \tag{2.7}$$

be obeyed far upstream, and that the flow far downstream be described by the conditions

$$\begin{aligned} &u_1 \to \gamma V_1, \quad v_1 \to 0, \quad T \to \frac{1}{V_2} + \frac{\lambda}{V_1}, \\ &u_2 \to V_2, \quad v_2 \to 0, \quad M \to \frac{1}{V_2} \quad \text{as } x \to \infty . \end{aligned} \tag{2.8}$$

The conditions (2.8), which are to be satisfied asymptotically far downstream, involve the unknown dimensionless velocity coefficients V_1 and V_2 shown in Fig. 1. These are related to the unknown Froude number F_2 and depth ratio λ through the conditions (2.3) and (2.5) at the two free boundaries. Substituting the downstream values from (2.8) into equation (2.3)

and solving for F_2 gives one relationship between the unknown parameters in the form

$$F_2^2 = \frac{2(\lambda + 1 - \lambda/V_1 - 1/V_2)}{\gamma^2(V_1^2 - 1)} \,. \tag{2.9}$$

Another relation comes from using the downstream conditions (2.8) in the interfacial condition (2.5), and may be written

$$\frac{1}{2} D\gamma^2 F_2^2(V_1^2 - 1) - \frac{1}{2} F_2^2(V_2^2 - 1) + (D - 1)\left(\frac{1}{V_2} - 1\right) = 0 \,. \tag{2.10}$$

The problem is thus completely defined by the conditions (2.1)–(2.10).

At this stage, it is convenient to introduce the complex variable $z = x + \mathrm{i}y$. It is a consequence of the Cauchy–Riemann equations (2.1) that complex velocity potentials $w_j = \phi_j + \mathrm{i}\psi_j$, $j = 1, 2$ may be introduced, which are analytic functions of the spatial variable z. Following Forbes and Schwartz [10], a new complex spatial variable $\zeta = \xi + \mathrm{i}\eta$ is now defined, such that the bottom maps to the straight line $\eta = 0$ in this new ξ, η coordinate system. This transformation, although not strictly necessary, nevertheless enhances the efficiency of the numerical solution to be described in Section 4. The required conformal mapping is the familiar Joukowski transformation

$$\zeta = \frac{1}{2}\left(z + \frac{\alpha^2}{z}\right) . \tag{2.11}$$

Equation (2.11) may be inverted to yield

$$z = \zeta + (A + \mathrm{i}B) \,, \tag{2.12a}$$

in which

$$A + \mathrm{i}B = [\zeta^2 - \alpha^2]^{1/2} \,. \tag{2.12b}$$

In these new coordinates, the bottom condition (2.2) becomes simply

$$\frac{\partial \phi_2}{\partial \eta} = 0 \quad \text{on } \eta = 0 \,. \tag{2.13}$$

In view of the fact that the complex velocity potentials $w_j = \phi_j + \mathrm{i}\psi_j$, $j = 1, 2$ are analytic functions of the variable $\zeta = \xi + \mathrm{i}\eta$, it is possible to derive integrodifferential equations relating the real and imaginary parts of the functions $\mathrm{d}w_j/\mathrm{d}\zeta$, $j = 1, 2$, along the two free boundaries of the fluids. This is done with the aid of Cauchy's integral formula in each fluid layer. To begin, the free surface of the upper fluid (layer 1) is parametrized using an arclength s_1, and the interfacial surface between layers 1 and 2 is parametrized by arclength s_2. Thus, along each free boundary,

$$\left(\frac{\mathrm{d}\xi}{\mathrm{d}s_j}\right)^2 + \left(\frac{\mathrm{d}\eta}{\mathrm{d}s_j}\right)^2 = 1 \,, \quad j = 1, 2 \,. \tag{2.14}$$

The kinematic condition (2.4) on the free surface becomes

$$\frac{\mathrm{d}\psi_1}{\mathrm{d}s_1} = 0\,, \tag{2.15}$$

and the two kinematic conditions (2.6) at the interface may be written

$$\frac{\mathrm{d}\psi_j}{\mathrm{d}s_2} = 0 \quad j = 1, 2\,, \tag{2.16}$$

reflecting the fact that each free boundary is a fluid streamline. The Bernoulli equation (2.3) at the free surface of fluid layer 1 may be written in terms of the arclength s_1 parametrizing this surface, and in the new ξ–η coordinate system, transforms to

$$\frac{1}{2} F_2^2 \frac{A^2 + B^2}{[(\xi + A)^2 + (\eta + B)^2]} \left(\frac{\mathrm{d}\phi_1}{\mathrm{d}s_1}\right)^2 + \eta + B$$
$$= \tfrac{1}{2}\gamma^2 F_2^2 + \lambda + 1\,, \tag{2.17}$$

in which the functions A and B are defined by equation (2.12b). On the interface between fluid layers 1 and 2, the dynamic condition (2.5) becomes

$$\frac{1}{2} F_2^2 \frac{A^2 + B^2}{[(\xi + A)^2 + (\eta + B)^2]} \left[D\left(\frac{\mathrm{d}\phi_1}{\mathrm{d}s_2}\right)^2 - \left(\frac{\mathrm{d}\phi_2}{\mathrm{d}s_2}\right)^2\right] + (D-1)(\eta + B)$$
$$= \tfrac{1}{2} D\gamma^2 F_2^2 - \tfrac{1}{2} F_2^2 + D - 1\,. \tag{2.18}$$

The integrodifferential equation relating the real and imaginary parts of the function $\mathrm{d}w_2/\mathrm{d}\zeta$ in the lower fluid (layer 2) along the internal interface may now be derived with the aid of Cauchy's integral formula. This development follows closely that given by Forbes and Schwartz [10] and Forbes [7]. Fluid layer 2 is first extended by reflection about the horizontal bottom $\eta = 0$ to form an image layer 2 with an image free boundary, lying beneath the actual river bed $\eta = 0$. Values of the dependent variable $w_2(\zeta)$ in this image fluid are related to values in the actual layer 2 by means of the reflection condition

$$\bar{w}_2(\bar{\zeta}) = w_2(\zeta)\,, \tag{2.19}$$

which is a consequence of the bottom condition (2.13), and satisfies it identically. Here, the bars denote complex conjugation.

Cauchy's integral formula is applied to the complex function

$$\chi_2(\zeta) = \frac{\mathrm{d}w_2}{\mathrm{d}\zeta} - 2\,,$$

and may be written

$$\oint_\Gamma \frac{\chi_2(\zeta)\,\mathrm{d}\zeta}{\zeta - \zeta(s_2)} = 0\,, \tag{2.20}$$

where the path Γ consists of the entire interfacial free surface with a semi-circular path of vanishingly small radius excluding the point $\zeta(s_2)$, the entire image free surface, and vertical lines $\xi = \pm L$, as $L \to \infty$, connecting the two surfaces. The integration variable ζ in equation

(2.20) represents any point on the contour Γ. In the limit $L\to\infty$, the contributions from the two vertical lines become zero. If σ_2 is the value of arclength at some moveable point $\zeta(\sigma_2)$ along the interfacial free surface, then the corresponding point on the image free surface is $\bar{\zeta}(\sigma_2)$, and equation (2.20) yields

$$i\pi\chi_2(\zeta(s_2)) = -\int_{-\infty}^{\infty} \frac{\chi_2(\zeta(\sigma_2))\zeta'(\sigma_2)}{\zeta(\sigma_2)-\zeta(s_2)}\,d\sigma_2 + \int_{-\infty}^{\infty} \frac{\chi_2(\bar{\zeta}(\sigma_2))\bar{\zeta}'(\sigma_2)}{\bar{\zeta}(\sigma_2)-\zeta(s_2)}\,d\sigma_2\,. \tag{2.21}$$

The first integral in equation (2.21) is singular in the Cauchy principal-value sense as $\sigma_2\to s_2$. It now remains to take the imaginary part of this equation, making use of the reflection condition (2.19) to eliminate quantities at the image surface in favour of their values at the true interfacial free surface, to give the desired integrodifferential equation in the form

$$\begin{aligned}&\pi[\phi_2'(s_2)\xi'(s_2)-2]\\ &\quad=\int_{-\infty}^{\infty}\frac{[\phi_2'(\sigma_2)-2\xi'(\sigma_2)][\eta(\sigma_2)-\eta(s_2)]+2\eta'(\sigma_2)[\xi(\sigma_2)-\xi(s_2)]}{[\xi(\sigma_2)-\xi(s_2)]^2+[\eta(\sigma_2)-\eta(s_2)]^2}\,d\sigma_2\\ &\qquad+\int_{-\infty}^{\infty}\frac{[\phi_2'(\sigma_2)-2\xi'(\sigma_2)][\eta(\sigma_2)+\eta(s_2)]+2\eta'(\sigma_2)[\xi(\sigma_2)-\xi(s_2)]}{[\xi(\sigma_2)-\xi(s_2)]^2+[\eta(\sigma_2)+\eta(s_2)]^2}\,d\sigma_2\,,\end{aligned} \tag{2.22}$$

in which the kinematic condition (2.16) has been employed (with $j=2$). The derivation of a similar equation for a fluid of infinite depth has been detailed by Forbes [7].

Essentially the same methods outlined above are used to derive integrodifferential equations relating the real and imaginary parts of the function $dw_1/d\zeta$ along the free boundaries of fluid layer 1. Since there is both an upper free surface and a lower interfacial free boundary to layer 1, there will be two such integrodifferential equations in this layer. Each such equation involves values of the unknown functions on both free boundaries, although the two equations are linearly dependent. Using the symbol σ_1 to denote the value of the arclength along the upper free surface at a moveable point $\zeta(\sigma_1)$, the two integrodifferential equations in layer 1 may be derived in the form

$$\begin{aligned}&\pi[\phi_1'(s_j)\xi'(s_j)-2\gamma]\\ &\quad=-\int_{-\infty}^{\infty}\frac{[\phi_1'(\sigma_2)-2\gamma\xi'(\sigma_2)][\eta(\sigma_2)-\eta(s_j)]+2\gamma\eta'(\sigma_2)[\xi(\sigma_2)-\xi(s_j)]}{[\xi(\sigma_2)-\xi(s_j)]^2+[\eta(\sigma_2)-\eta(s_j)]^2}\,d\sigma_2\\ &\qquad+\int_{-\infty}^{\infty}\frac{[\phi_1'(\sigma_1)-2\gamma\xi'(\sigma_1)][\eta(\sigma_1)-\eta(s_j)]+2\gamma\eta'(\sigma_1)[\xi(\sigma_1)-\xi(s_j)]}{[\xi(\sigma_1)-\xi(s_j)]^2+[\eta(\sigma_1)-\eta(s_j)]^2}\,d\sigma_1\,,\quad j=1,2\,.\end{aligned} \tag{2.23}$$

The first integral in this equation is taken along the interfacial surface and is singular in the Cauchy principal-value sense when $j=2$, and the second integral is taken along the upper free surface and is singular when $j=1$.

The calculation of the shapes of the two free boundaries and the unknown constants F_2 and λ thus consists of finding a solution to the integrodifferential equations (2.22) and (2.23) coupled with the dynamic conditions (2.17) and (2.18) and the relations (2.9) and (2.10). These are subject to the additional requirements (2.14) for the two arclengths and the

asymptotic conditions (2.7) and (2.8) appropriately transformed to the ξ–η coordinate system by means of the mapping (2.11).

3. Shallow-water approximation

Some insight into the nature of transcritical flow in the case of a two-layer system can be gained by use of the shallow water, or long wave, approximation to the full system of hydrodynamic equations. This has been done by Armi [2], Benton [4] and Wood and Lai [18], for example, and for ease of reference we summarize the results here. In particular, it will be seen that shallow-water theory leads to an approximate definition of critical flow for a two-layer system (equation (3.7)), which is useful in discussing solutions to the fully non-linear problem.

We return briefly to dimensional variables as described at the beginning of Section 2. In the top layer of fluid, shallow-water theory yields the approximate mass- and momentum-conservation equations in the form

$$\begin{aligned} &u_1(T-M) = c_1 H_1 \,, \\ &\tfrac{1}{2}u_1^2 + gT = \tfrac{1}{2}c_1^2 + g(H_1 + H_2) \,, \end{aligned} \tag{3.1}$$

and the same conservation laws in the bottom layer of fluid can be written

$$\begin{aligned} &u_2(M-h) = c_2 H_2 \,, \\ &\tfrac{1}{2}u_2^2 + (1-D)gM + DgT = \tfrac{1}{2}c_2^2 + (1-D)gH_2 + Dg(H_1 + H_2) \,, \end{aligned} \tag{3.2}$$

where D is the ratio of the fluid density in the top layer 1 to the density in layer 2, as before.

It is convenient, as in Section 2, to define upstream Froude numbers in each layer. Thus, far upstream in the top layer the flow is characterized by Froude number $F_1 = c_1(gH_1)^{-1/2}$, and in the bottom layer the Froude number far upstream is $F_2 = c_2(gH_2)^{-1/2}$. In addition, we shall also define *local* Froude numbers

$$f_1 = \frac{u_1}{[g(T-M)]^{1/2}} \,, \qquad f_2 = \frac{u_2}{[g(M-h)]^{1/2}} \tag{3.3}$$

which vary at each section x along the channel, but approach the upstream Froude numbers F_1 and F_2 as $x \to -\infty$. The use of the mass-conservation equations in each fluid layer (the first equation in each of (3.1) and (3.2)) enables the horizontal velocity components u_1 and u_2 to be written

$$u_j = [c_j H_j g f_j^2]^{1/3} \,, \quad j = 1, 2 \,, \tag{3.4a}$$

and the elevations $T(x)$ and $M(x)$ of the surface and interface to be expressed as

$$M(x) = h(x) + \left[\frac{c_2^2 H_2^2}{f_2^2 g}\right]^{1/3} \,, \qquad T(x) = M(x) + \left[\frac{c_1^2 H_1^2}{f_1^2 g}\right]^{1/3} \,. \tag{3.4b}$$

The results derived in equations (3.4) are now substituted into the momentum-conservation equations (the second equation in each of (3.1) and (3.2)), to yield the system

$$\begin{aligned}
&\frac{1}{2}f_1^{4/3}+\frac{h/H_2}{\lambda F_1^{2/3}}+\frac{1}{(\gamma\lambda f_2)^{2/3}}+\frac{1}{f_1^{2/3}}=\frac{1}{2}F_1^{4/3}+\frac{1+1/\lambda}{F_1^{2/3}}\,,\\
&\frac{1}{2}f_2^{4/3}+\frac{h/H_2}{F_2^{2/3}}+\frac{1}{f_2^{2/3}}+D\left(\frac{\lambda\gamma}{f_1}\right)^{2/3}=\frac{1}{2}F_2^{4/3}+\frac{1+D\lambda}{F_2^{2/3}}\,,
\end{aligned}\tag{3.5}$$

in which the upstream speed ratio γ and depth ratio λ are as defined in Section 2.

Following Armi [2], the governing equations (3.5) are written in differentiated form according to the matrix equation

$$\begin{bmatrix} f_1^{1/3}(1-f_1^{-2}) & -(\gamma\lambda)^{-2/3}f_2^{-5/3} \\ -D(\gamma\lambda)^{2/3}f_1^{-5/3} & f_2^{1/3}(1-f_2^{-2}) \end{bmatrix}\begin{bmatrix} \partial f_1/\partial x \\ \partial f_2/\partial x \end{bmatrix}=-\frac{h'(x)}{H_2}\begin{bmatrix} 3(2\lambda F_1^{2/3})^{-1} \\ 3(2F_2^{2/3})^{-1} \end{bmatrix}.\tag{3.6}$$

Critical flow occurs when the bottom is horizontal, $h'(x)=0$, but at a section x where the matrix equation (3.6) does not possess a trivial solution. This can only occur when the determinant of the coefficient matrix in equation (3.6) is zero, giving rise to the 'critical' condition

$$f_C^2=f_1^2+f_2^2-f_1^2f_2^2+D=1\,,\tag{3.7}$$

which must be satisfied at the crest of the submerged obstacle responsible for the flow. Equation (3.7) shows that f_C is the appropriate combination Froude number for two-layer flows. As suggested by Armi [2], this Froude number f_C is expected to be greater than one far upstream, to pass through the critical value 1 at the crest of the weir, and then to fall below one far downstream, although the individual Froude numbers f_1 and f_2 in each fluid layer may always exceed unity, in this approximation.

4. The numerical solution

The numerical method used for the approximate solution of the equations of motion derived in Section 2 is based on that presented by Forbes and Schwartz [10] and extended to a more general class of problems by Forbes [7]. It is therefore only necessary to present a brief overview of this technique here.

Each free boundary is represented as a discrete set of grid points in some appropriate 'window' of finite width including the semi-circular weir. The points are chosen to be equally spaced with respect to the arclength along each surface, so that the top free surface is represented by the set $\{s_k^{(1)}\}$, $k=1,2,\ldots,N$ with constant point spacing h_1, and the interfacial free surface is represented by points $\{s_k^{(2)}\}$, $k=1,2,\ldots,M$ having constant spacing h_2.

Newton's method is used to solve for a vector of unknowns of length $N+M-1$, made up from the derivatives $\eta'(s_k^{(1)})$, $k=2,\ldots,N$ and $\eta'(s_k^{(2)})$, $k=2,\ldots,M$ and the depth ratio λ. These derivatives correspond approximately to the slopes of each free boundary (in the ξ–η coordinate system) measured at the numerical grid points. To begin the Newtonian iteration, an initial guess is made for these unknown derivatives and for λ; in the absence of a better

guess supplied by some previously computed non-linear solution, we follow the suggestion of Forbes [9] and use

$$\eta'(s_2) \approx \left(\frac{1-V_2}{2V_2}\right) \frac{e^{\pi s_2/2}}{1+e^{\pi s_2}}, \qquad \eta'(s_1) \approx \left[\frac{1-V_2}{2V_2} + \frac{\lambda(1-V_1)}{2V_1}\right] \frac{e^{\pi s_1/2}}{1+e^{\pi s_1}}, \tag{4.1}$$

which are consistent with the upstream and downstream conditions (2.7) and (2.8). However, the true values of the constants V_1 and V_2 are as yet unknown, and so approximate values of about 1.5 are assumed. For the unknown depth ratio λ, an initial guess of about 0.5 is usually adequate.

Once an initial guess has been made for the derivatives in equation (4.1) and for λ, the computation of all other quantities at the two free boundaries is possible, based on this guess. The process begins by supplying values of the dependent variables at the two points furthest upstream on each surface, in accordance with the upstream conditions (2.7) and (2.8). Thus we take

$$\begin{aligned} &\eta'(s_1^{(j)}) = 0, \qquad \xi'(s_1^{(j)}) = 1, \qquad \xi(s_1^{(j)}) = s_1^{(j)}, \quad j = 1, 2, \\ &\eta(s_1^{(1)}) = \tfrac{1}{2}(1+\lambda), \qquad \eta(s_1^{(2)}) = \tfrac{1}{2} \end{aligned} \tag{4.2a}$$

and

$$\begin{aligned} &\phi_1(s_1^{(j)}) = 2\gamma\xi(s_1^{(j)}), \quad j = 1, 2, \\ &\phi_1'(s_1^{(2)}) = 2\gamma, \qquad \phi_2(s_1^{(2)}) = 2\xi(s_1^{(2)}). \end{aligned} \tag{4.2b}$$

The surface elevations η are next obtained for both free boundaries using the trapezoidal rule to integrate the functions η', with initial values supplied by (4.2a). Numerical values for the derivatives ξ' at the grid points along each surface may be computed immediately from equation (2.14), and these are likewise integrated using the trapezoidal rule to give approximate values of the functions $\xi(s_j)$, $j = 1, 2$.

The downstream conditions (2.8) are transformed into the ξ, η coordinate system and satisfied in part by requiring

$$V_2 = \frac{1}{2\eta(s_M^{(2)})}, \qquad V_1 = \frac{\lambda V_2}{2V_2\eta(s_N^{(1)}) - 1}, \tag{4.3}$$

from which the unknown downstream speed coefficients V_1 and V_2 are computed. The Froude number F_2 in layer 2 is now obtained from equation (2.9).

The dynamic condition (2.17) at the upper free surface is solved to yield the quantities $\phi_1'(s_k^{(1)})$, $k = 1, 2, \ldots, N$. These are integrated numerically using the trapezoidal rule, to provide an approximation to the function ϕ_1 at the upper surface, assuming an initial value given by equation (4.2b). This now completely determines the velocity potential ϕ_1 in the upper layer of fluid, along the upper free surface. In order to obtain this velocity potential along the interfacial free surface, the integrodifferential equation (2.23) is used with $j = 2$. The integrals in this equation are truncated upstream and downstream, so that attention is restricted to the finite intervals on each free boundary under consideration. Care must be taken, however, to estimate the portions of the integrals ignored in this truncation process,

otherwise unacceptably large numerical error may result. We assume that the flow outside the truncation 'window' is approximately uniform, so that the upstream and downstream portions of the integrals in (2.23) can be estimated using conditions (2.7) and (2.8). The integrodifferential equation is now evaluated at the half-points $s^{(2)}_{k-1/2}$, $k = 2, \ldots, M$, and the integrals are discretized using the trapezoidal rule and a result due to Monacella [13] that allows the Cauchy singularity in the integrand simply to be ignored. Values of ξ and η at the half-mesh points are expressed as the averages of values at the two neighbouring points. In view of equation (4.2b), the integrodifferential equation is thus replaced by a linear algebraic system of equations for the derivatives $\phi_1'(s_k^{(2)})$, $k = 2, \ldots, M$, which is solved (at each iteration of Newton's method) by Gaussian elimination. The function ϕ_1 at the interfacial free surface is then obtained by trapezoidal rule integration, using equation (4.2b) to supply the starting value at the first point upstream. Finally, the velocity potential ϕ_2 in the lower layer of fluid is evaluated at the interface by solving equation (2.18) for the derivatives $\phi_2'(s_k^{(2)})$, $k = 1, 2, \ldots, M$, and integrating these quantities using the trapezoidal rule and the upstream value taken from equation (4.2b).

The initial estimates for the derivatives of the surface height η at each free boundary and the depth ratio λ are improved iteratively, using Newton's method. When the integrodifferential equation (2.22) is truncated and discretized in the manner described above, it yields a system of $M - 1$ non-linear, algebraic equations. A further $N - 1$ non-linear equations come from the integrodifferential equation (2.23) at the top free surface ($j = 1$), after it has been similarly truncated and discretized. Equation (2.10) provides the final algebraic equation needed to close the system. The damped Newton's method detailed by Forbes and Schwartz [10] and Forbes [7] is then used to complete the numerical solution.

5. Presentation of results

In this section, the results of rather extensive computation are presented and analyzed. About 130 separate converged numerical solutions have been obtained, typically with 101 numerical grid points on each free boundary. This is usually sufficient to guarantee about three figures accuracy. All computer programs were run on the PYRAMID 9810 mini-computer in the Mathematics Department at the University of Queensland, and in general, five iterations of Newton's method and about ninety minutes of computer time were required to produce each solution. As outlined in Sections 2 and 4, the approach adopted was to specify the speed ratio γ and allow the upstream depth ratio λ to be obtained as part of the solution. This is equivalent to specifying the volume flow rates in each fluid layer, and allowing upstream conditions to be determined. In an alternative procedure, we have also developed a method in which the upstream depth ratio λ is assumed known and the speed ratio γ found numerically; although simpler to implement, this approach appears to yield results in a less convenient format, and accordingly, results obtained in this fashion will not be discussed further. However, the surface profiles in Fig. 1 were obtained by this method.

In Fig. 2, we present surface profiles obtained with $D = 1$ and $\gamma = 1$, for the two different values $\alpha = 0.25$ and $\alpha = 0.475$ of the dimensionless semi-circle radius. In this case, both the densities and the upstream fluid speeds are the same in each fluid layer, so that the system is indistinguishable from a single fluid layer of height $1 + \lambda$ flowing over a weir. This affords a valuable opportunity for comparison with the results of Forbes [9] for trans-critical flow in a single layer, and we find that the two sets of calculations are in agreement to at least three

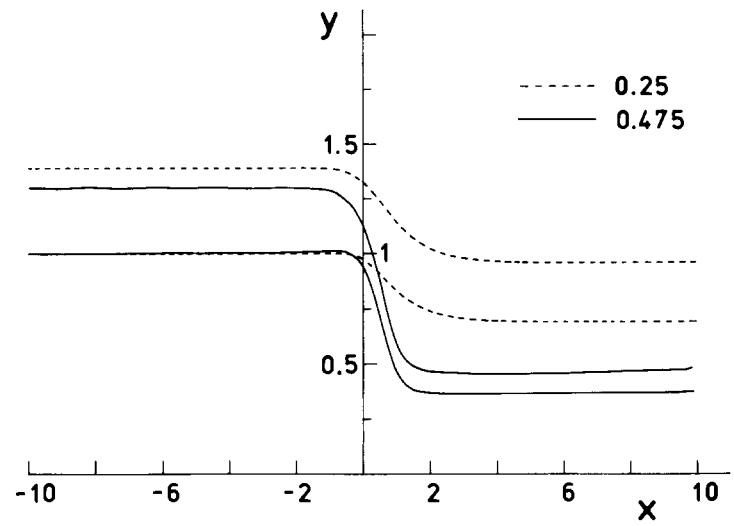

Fig. 2. Surface elevations for the case $D = 1$, $\gamma = 1$ and the two values of the semi-circle radius $\alpha = 0.25$ and $\alpha = 0.475$.

significant figures, when allowance is made for the fact that the effective upstream depth in the present problem is $1 + \lambda$. There is thus good reason for confidence in the correctness of the present numerical solution, in particular since Forbes [9] showed that the single-layer calculations were well confirmed by experiment.

Some remarks on the effects of numerical error in the solution profiles shown in Fig. 2 are appropriate. We have verified that the solutions are independent of the numerical point spacings h_1 and h_2, by varying these intervals and observing that the solutions are unaffected to at least graphical precision. There is, however, a small error caused by the truncation of the domains of the integrodifferential equations (2.22) and (2.23) to the numerical 'window' described in Section 4. The upstream truncation results in the generation of numerical wavelets of very small amplitude ahead of the weir; such non-physical waves are present in the upstream portions of Fig. 2, but may be too small to be visible. They have no discernible effect upon the rest of the solution, and as they are discussed in detail by Forbes and Schwartz [10], they will not be considered further here. The downstream truncation of the integrodifferential equations has a very small effect upon the last few downstream grid points, resulting in a slight upward inflexion of the surface there. This effect is also present in Fig. 2, but may again be too small to be seen.

Figure 3 shows how the upstream Froude numbers F_1 and F_2 in layers 1 and 2, respectively, vary with the semi-circle radius α, for the same case $D = 1$, $\gamma = 1$ discussed in Fig. 2. In addition, we have also plotted the upstream combination Froude number F_C for the two-fluid system, which is obtained from equation (3.7) as

$$F_C^2 = F_1^2 + F_2^2 - F_1^2 F_2^2 + D \,. \tag{5.1}$$

For small α, the predictions of shallow-water theory are confirmed. The combination Froude number F_C far upstream exceeds unity, as in fact do both the individual Froude numbers F_1 and F_2 in each fluid layer. The combination Froude number passes through the critical value on some curve in the vicinity of the weir, and becomes subcritical ($f_C < 1$) far downstream.

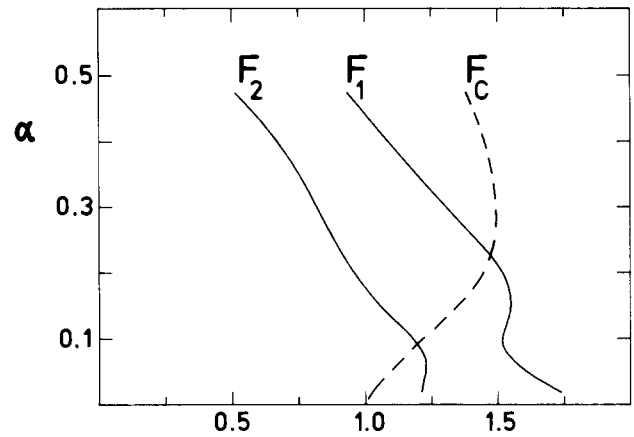

Fig. 3. The upstream Froude numbers F_1 and F_2 in the top and bottom layers and the upstream combination Froude number F_C, as functions of semi-circle radius α, for $D = 1$ and $\gamma = 1$.

As the semi-circle radius α is increased, however, the simple shallow-water theory becomes less reliable, since in particular, the quantity f_C^2 far downstream eventually becomes negative for sufficiently large α, as revealed by our numerical algorithm, showing that the combination Froude number defined in equation (3.7) is no longer adequate to describe the whole flow. In addition, the upstream Froude numbers F_1 and F_2 in each layer can fall below one, although these Froude numbers both exceed one far downstream. Thus, in addition to the overall flow being transcritical in the sense that the combination Froude number f_C passes through the critical value (as in equation (3.7)), transcritical flow may also be occurring in either or both of the separate fluid layers. The numerical scheme fails to yield a solution for $\alpha > 0.475$, since the downstream portions of the flow become very fast and shallow for such large disturbance sizes, giving rise in effect to a downstream flow which is numerically and physically unstable.

Surface profiles are shown for the case $D = 0.6$, $\gamma = 1$ in Fig. 4, for two different values of the semi-circle radius, $\alpha = 0.2$ and $\alpha = 0.425$. There is little qualitative difference between the surface profiles in this case and those obtained with $D = 1$ shown in Fig. 2, and the same remarks concerning the numerical accuracy and the effects of truncation apply here also. Again it is found that the numerical method does not converge for values of α larger than 0.425, since the downstream portion of the top layer of fluid, in particular, has become very shallow and flows very rapidly, giving rise to a flow which is effectively unstable both numerically and physically.

Figure 5 details the behaviour of the upstream Froude numbers F_1 and F_2 in each fluid layer as the semi-circle radius α is increased, for the case $D = 0.6$, $\gamma = 1$ considered in Fig. 4. In addition, the upstream combination Froude number F_C defined in equation (5.1) is also shown for this case. The qualitative behaviour is very similar to that shown in Fig. 3 for $D = 1$, except that the curves for F_1 and F_2 in this case are more nearly monotonic, and less undulatory. As described previously, the predictions of shallow-water theory are confirmed for small α, but as α increases, this approximate theory is no longer adequate to describe the overall flow.

The variation of the upstream combination Froude number F_C with circle radius α is shown in Fig. 6, for the three different values $D = 0.3$, $D = 0.6$ and $D = 1$ of the density ratio. In each case, $F_C \to 1$ as $\alpha \to 0$, which is to be expected on the basis of shallow-water

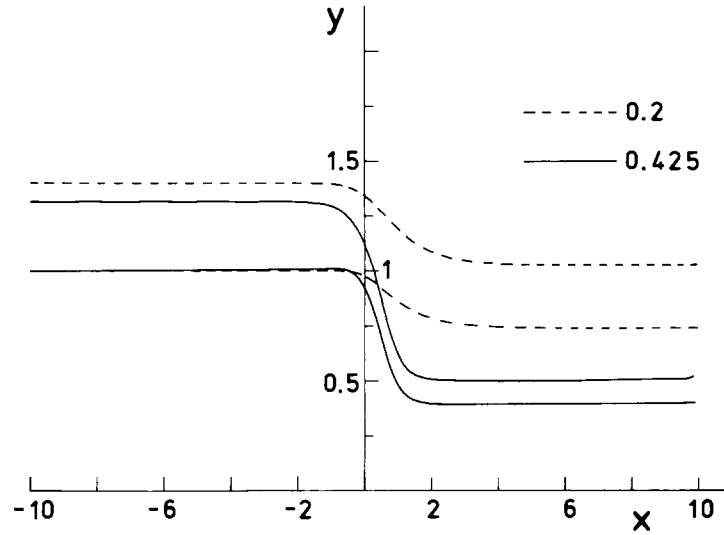

Fig. 4. Surface elevations for the case $D = 0.6$, $\gamma = 1$ and the two values of the semi-circle radius $\alpha = 0.2$ and $\alpha = 0.425$.

theory, since the requirement of critical flow at the obstruction (see equation (3.7)) implies that the uniform flow conditions which must exist as $\alpha \to 0$ necessarily occur at the critical value of the combination Froude number. As α is increased, we find that the Froude number F_C first increases to a maximum and then decreases until the point where the numerical scheme fails to converge, for every non-zero value of the density ratio D.

A more detailed study of the influence of the density ratio D upon the solutions is summarized in Fig. 7. Here, the upstream Froude numbers F_1 and F_2 in each fluid layer and the upstream combination Froude number F_C are plotted against the density ratio D, for the case in which the semi-circle radius and the upstream speed ratio are held fixed at the values $\alpha = 0.2$ and $\gamma = 1$, respectively. For $D > 1$, we are apparently unable to find a stable solution, which is to be expected since the upper fluid would then be heavier than the lower one. The curves in Fig. 7 were sketched by obtaining a solution for $D = 1$, and then using

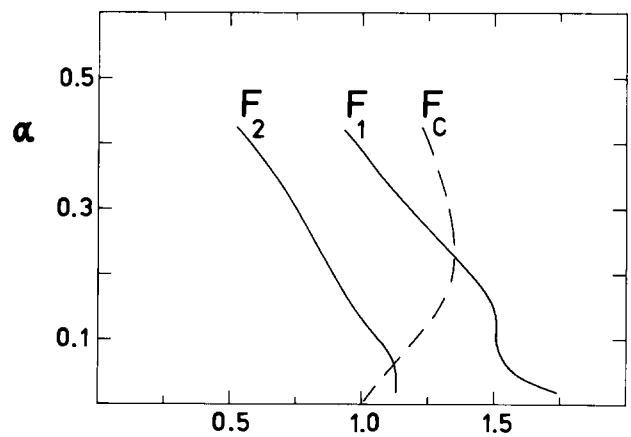

Fig. 5. The upstream Froude numbers F_1 and F_2 in the top and bottom layers and the upstream combination Froude number F_C, as functions of semi-circle radius α, for $D = 0.6$ and $\gamma = 1$.

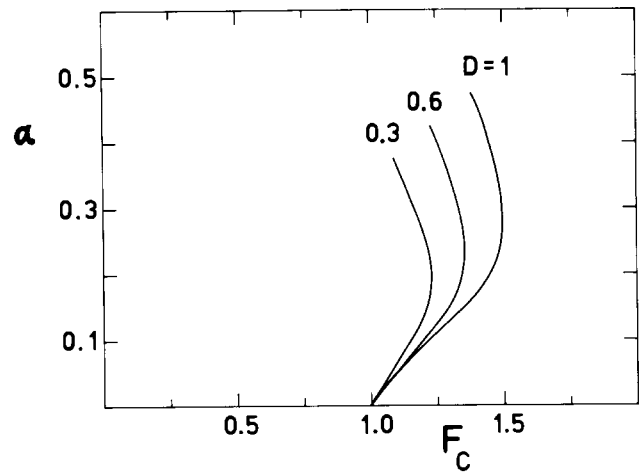

Fig. 6. The upstream combination Froude number F_C as a function of semi-circle radius α, for the three values of the density ratio $D = 0.3$, $D = 0.6$, and $D = 1$. The upstream speed ratio is $\gamma = 1$.

this as the initial guess for a solution at a slightly smaller values of D, and proceeding incrementally in this way until a solution was eventually obtained with $D = 0$. Clearly each of the upstream Froude numbers shown in Fig. 7 decreases monotonically as D is reduced from its maximum value 1 to its minimum 0.

An interesting situation arises when $D = 0$, which may be considered as a singular or degenerate value of the density ratio D. In this singular case, the upper fluid effectively has zero weight relative to the fluid in the lower layer, and so the lower fluid behaves independently of the upper one. This is reflected by the equations governing the behaviour of the fluid in each layer, which de-couple at the value $D = 0$. In the above discussion of the results presented in Fig. 7, it was explained that a solution was obtained at $D = 0$ as the numerical limit of the branch of solutions which exist for non-zero D. It turns out that a different solution may be obtained for $D = 0$ at the *same* values of the other parameters α and γ, simply by altering the initial guess supplied to the Newtonian iteration scheme described in Section 4, and we have used equation (4.1) for this purpose.

Figure 8 shows the two different solutions computed in this way for the singular case $D = 0$, with semi-circle radius $\alpha = 0.2$ and upstream speed ratio $\gamma = 1$. For each of the two

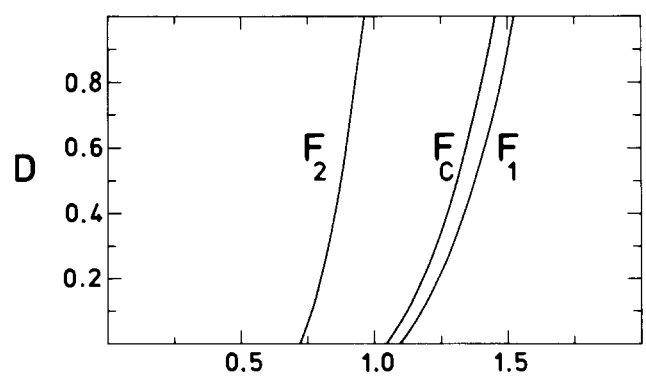

Fig. 7. The upstream Froude numbers F_1 and F_2 in the top and bottom layers and the upstream combination Froude number F_C, as functions of the density ratio D, for $\alpha = 0.2$ and $\gamma = 1$.

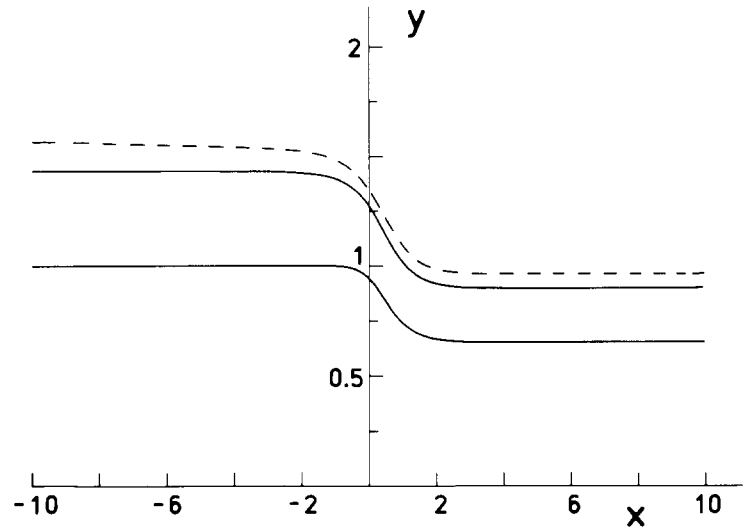

Fig. 8. Surface elevations for two different solution types at the same values of $\alpha = 0.2$ and $\gamma = 1$, for the singular case $D = 0$. The surfaces for one of the solution types are sketched with a dashed line, and the other solution type is indicated by a solid line. The interfacial free surface is the same for both solution types.

different solution types, the interface between layer 1 and layer 2 has exactly the same location, which is to be expected as the fluid in the lower layer is unaffected by the presence of the upper fluid. In fact, the lower fluid flows as an independent single-layer system, and as such may be compared with the results of Forbes [9], with which it is in good agreement. In the upper layer of fluid, however, there is evidently a lack of uniqueness associated with the upstream depth ratio λ, so that the upper fluid can flow at two different depths, when the speed ratio γ is fixed.

6. Discussion and conclusions

Steady flow of a system of two ideal fluids over a semi-circular weir has been investigated, using a numerical scheme capable of solving the fully non-linear two-dimensional equations of motion. The flow is of the trans-critical type, by which it is meant that the combination Froude number for the two-fluid system passes through the critical value 1 near the weir. The solution consists of a wave-free region of uniform flow both upstream and downstream of the semi-circular obstruction; these two regions are of different depths, and so are connected by a waterfall-like flow over the obstacle.

Solutions have been found for values of the ratio D of the fluid density in the upper layer to that in the lower layer in the interval $0 \leq D \leq 1$. When $D > 1$, stable solutions are apparently not possible, since the upper fluid would then be heavier than the lower fluid, precluding a steady solution. When $D = 1$ and the upstream speed ratio γ is also 1, the system is indistinguishable from a single-layer flow over a weir, and so can be compared with the theoretical and experimental results of Forbes [9], with which it is in agreement. As D decreases toward zero, the solution properties change smoothly, and at the value $D = 0$, the lower layer of fluid behaves as a single fluid system, since it is unaffected by the presence of the upper layer. Thus the properties of the fluid in the lower layer may again be compared with the results of Forbes [9], and agreement is found to be good.

At the singular value $D = 0$, the fluid in each layer behaves independently of the other. Although the bottom layer of fluid is forced to flow as a single fluid system with properties described by Forbes [9], the upper layer of fluid is evidently capable of two different flow behaviour types. For one of these solution types, it happens that the Froude number f_1 in the upper layer is always greater than 1, increasing steadily from its supercritical upstream value F_1 to a larger supercritical downstream value. For the other solution type, the upstream Froude number F_1 in the top fluid layer is subcritical ($F_1 < 1$), the flow passes through the critical value $f_1 = 1$ at some point upstream of the weir and then becomes supercritical far downstream. We have attempted to continue this second solution type at $D = 0$ into the $D > 0$ portion of the parameter space, but find that the numerical method is only capable of obtaining such solutions in a very small interval near $D = 0$, for a reason which is presently not understood. However, it is clear that the singular value $D = 0$ is associated with a lack of uniqueness. Indeed, there may exist other solutions in a neighbourhood of $D = 0$, although our numerical scheme has so far only detected the two types discussed above.

As stated in the introduction, there are many different possible solution branches in the case of flow of a single layer of fluid over a weir, of which the trans-critical solution type is only one possible outcome. Other solution types may involve downstream waves, or a symmetric upstream and downstream region free of waves, as discussed by Forbes and Schwartz [10] and Vanden-Broeck [16]. Surely the same complexity of solution branches must also exist in the case of a two-fluid system, so that solutions with downstream waves on both free surfaces must be considered a possibility, for example. In addition, extra complexity may exist for a two-fluid system, for which there is no equivalent in the single-fluid case. For example, the lower fluid could flow trans-critically while the upper fluid possessed downstream waves, and so on. Clearly a comprehensive study of all these possibilities lies well outside the scope of the present investigation, and awaits future elucidation.

References

1. J.M. Aitchison, A variable finite element method for the calculation of flow over a weir, Rutherford Laboratory report No. RL-79-069 (1979).
2. L. Armi, The hydraulics of two flowing layers with different densities, *J. Fluid Mech.* 163 (1986) 27–58.
3. L. Armi and D.M. Farmer, Maximal two-layer exchange through a contraction with barotropic net flow, *J. Fluid Mech.* 164 (1986) 27–51.
4. G.S. Benton, The occurrence of critical flow and hydraulic jumps in a multi-layered fluid system, *J. Met.* 11 (1954) 139–150.
5. P. Bettess and J.A. Bettess, Analysis of free surface flows using isoparametric finite elements, *Int. J. Num. Meth. Eng.* 19 (1983) 1675–1689.
6. D.M. Farmer and L. Armi, Maximal two-layer exchange over a sill and through the combination of a sill and contraction with barotropic flow, *J. Fluid Mech.* 164 (1986) 53–76.
7. L.K. Forbes, On the effects of non-linearity in free-surface flow about a submerged point vortex, *J. Eng. Math.* 19 (1985) 139–155.
8. L.K. Forbes, A numerical method for non-linear flow about a submerged hydrofoil, *J Eng. Math.* 19 (1985) 329–339.
9. L.K. Forbes, Critical free-surface flow over a semi-circular obstruction, *J. Eng. Math.* 22 (1988) 3–13.
10. L.K. Forbes and L.W. Schwartz, Free-surface flow over a semicircular obstruction, *J. Fluid Mech.* 114 (1982) 299–314.
11. F.M. Henderson, *Open Channel Flow*, Macmillan and Co., New York (1966).
12. W.K. Melville and K.R. Helfrich, Transcritical two-layer flow over topography, *J. Fluid Mech.* 178 (1987) 31–52.

13. V.J. Monacella, On ignoring the singularity in the numerical evaluation of Cauchy Principal Value integrals, Hydromechanics Laboratory research and development report 2356, David Taylor Model Basin, Washington D.C. (1967).
14. P.M. Naghdi and L. Vongsarnpigoon, The downstream flow beyond an obstacle, *J. Fluid Mech.* 162 (1986) 223–236.
15. N.S. Sivakumaran, T. Tingsanchali and R.J. Hosking, Steady shallow flow over curved beds, *J. Fluid Mech.* 128 (1983) 469–487.
16. J.-M. Vanden-Broeck, Free-surface flow over an obstruction in a channel, *Phys. Fluids* 30 (1987) 2315–2317.
17. J.-M. Vanden-Broeck and J.B. Keller, Weir flows, *J. Fluid Mech.* 176 (1987) 283–293.
18. I.R. Wood and K.K. Lai, Flow of layered fluid over broad crested weir, *J. Hyd. Div. ASCE* 98 (1972) 87–104.